J Radioanal Nucl Chem (2015) 303:681–691
DOI 10.1007/s10967-014-3472-8

Adsorption behavior of actinides and some typical fission products by silica/polymer-based *iso*Hex-BTP adsorbent from nitric acid solution

Ruiqin Liu · Shunyan Ning · Xinpeng Wang · Yuezhou Wei · Jinling Yang · Yaping Zhao · Youqian Ding · Jianhui Lan · Weiqun Shi

Received: 11 May 2014 / Published online: 9 September 2014

Abstract The silica/polymer-based *iso*Hex-BTP adsorbent (*iso*Hex-BTP/SiO_2-P) was prepared for partitioning Am(III) and Cm(III) from HLLW. Batch adsorption results showed that *iso*Hex-BTP/SiO_2-P exhibited high affinity and selectivity for Am(III) and Pu(IV) over U(VI), Ln(III) and other typical fission products in 3 mol dm^{-3} nitric acid. The effects of contact time, initial Dy(III) concentration and temperature on the adsorption of Dy(III) [as a simulated element of MA(III) and a representative element of Ln(III)] by *iso*Hex-BTP/SiO_2-P in 3 mol dm^{-3} nitric acid were investigated. The adsorption of Dy(III) fitted well to the pseudo-second-order kinetic model and the Langmuir isotherm model. The adsorption thermodynamic parameters revealed that the adsorption was a spontaneous, endothermic and entropy-driving process.

Keywords *Iso*Hex-BTP/SiO_2-P · Extraction chromatography · HLLW · Actinides · Lanthanides · Fission products

R. Liu · S. Ning · X. Wang · Y. Wei (✉)
School of Nuclear Science and Engineering, Shanghai Jiao Tong University, 800 Dongchuan Road, Shanghai 200240, China
e-mail: yzwei@sjtu.edu.cn

J. Yang · Y. Zhao · Y. Ding
Department of Radiochemistry, China Institute of Atomic Energy, Beijing 102413, China

J. Lan · W. Shi
Institute of High Energy Physics, Chinese Academy of Sciences, 19B YuquanLu,Shijingshan District, Beijing 100049, China

Introduction

The so-called minor actinides, americium, curium and neptunium, as well as a small amount of residual plutonium are the most important long-lived radionuclides, which are responsible for the long-term radiation hazards of vitrified high level liquid waste (HLLW) arising from the PUREX process [1–3]. Separating and transmuting them to short-lived or stable nuclides prior to the vitrification step could have a significant beneficial impact on bringing down the surveillance period from millions of years to a few hundred years. The selective separation of trivalent minor actinides [MA(III): Am(III) and Cm(III)] from the trivalent lanthanides (Ln(III)) which are present being about 20 up to 50 times more abundant than MA(III) in HLLW [3, 4] is important in P & T (Partitioning and Transmutation) strategy since some of the lanthanides exhibit large neutron-capture cross-sections, hence reducing transmutation efficiency of the minor actinides [5]. However, MA(III)-Ln(III)-separation is a challenging task that remains to be solved owing to their similar coordination chemistry and their disadvantageous ratio of presence in HLLW [4, 6, 7]. Currently, several two-step partitioning processes based on liquid–liquid extraction have been designed: the minor actinides and lanthanides are firstly co-extracted from the bulk of the fission products using oxygen donor ligands, e.g. CMPO [8], DMDOHEMA [9], TRPO [10] and DIDPA [11] in TRUEX [12], DIAMEX [12], TRPO [10] and DIDPA [11] processes, and subsequently the minor actinides could be selectively separated from the lanthanides using nitrogen or sulfur donor ligands in SANEX [1, 13, 14], CYANEX 301 [15, 16] processes, etc. Among various nitrogen or sulfur donor ligands, 2,6-bis(5,6-dialkyl-1,2,4-triazin-3-yl) pyridines (known as BTPs) turn out to be highly selective extractants for MA(III) over Ln(III) from

highly acidic solutions ($HNO_3 > 1$ mol dm^{-3}) [17]. They fulfill CHON principle, i.e., the species consist entirely of carbon, hydrogen, oxygen, and nitrogen atoms to make them combustible to safe gaseous products [18, 19]. So, many researches predominantly in Europe have been focused on the design of nitrogen-donor ligands for MA(III) separation [1, 7, 20]. However, a potential process application requires selectivity, fast kinetics, stability, high solubility and loading capacity [5]. The extracting agents BTPs available so far suffer from one or more drawbacks in liquid–liquid extraction system [5, 21], which might result in generating a great amount of organic waste and requiring extensive equipment for the multi-stage extraction, stripping and solvent-washing processes [22]. This requires further optimization to comply with process constrains. Therefore, a series of BTP derivatives where C–H bonds in the α-positions of the triazinyl rings are replaced by C–C bonds have been developed to increase the stability of this kind of ligands against hydrolysis and radiolysis as well as to improve the extracted capacity and the strip performance of MA(III) [5, 6]. On the other hand, these drawbacks can be alleviated by use of alternative techniques such as extraction chromatography and liquid membrane method [22–24]. Extraction chromatographic technique combines the selectivity of liquid–liquid extraction with the ease of operation of column chromatography for the clean separation of MA(III) [15, 25–27]. Furthermore, the feed for the PUREX process produced by dissolving commercial spent fuel (45.2 GWd tM^{-1}) in 4 mol dm^{-3} HNO_3 contained 131,917 μg g^{-1} U, 1,153 μg g^{-1} Pu, 24 μg g^{-1} ^{243}Am and 6 μg g^{-1} ^{244}Cm [3], therefore, compared to uranium and plutonium, the minor actinides are significantly less abundant in the spent fuel indicating that the scale of the separation process for minor actinides from HLLW should be considerably smaller than that of a main separation process such as PUREX [28, 29].

As an alternative technology of the liquid–liquid extraction process, we have reported a direct separation process of MA(III) from HLLW based on extraction chromatography (Fig. 1) [29, 30]. The process uses a single-column packed with silica/polymer-based BTP adsorbent named as BTP/SiO_2-P, e.g. *iso*Hex-BTP/SiO_2-P [*iso*Hex-BTP: 2,6-bis(5,6-di*iso*hexyl)-1,2,4-triazin-3-yl)pyridine]. The extraction chromatographic material, *iso*Hex-BTP/SiO_2-P adsorbent, using silica/polymer composite support (SiO_2-P) as the inert support and *iso*Hex-BTP as the extracting agent, was prepared. SiO_2-P support contains a macroreticular styrene–divinylbenzene copolymer which is immobilized in porous silica particles with pore size of 0.6 μm and mean diameter of 60 μm. The content of extracting agent *iso*Hex-BTP in *iso*Hex-BTP/SiO_2-P adsorbent was relatively high (up to 33.3 % of the total mass

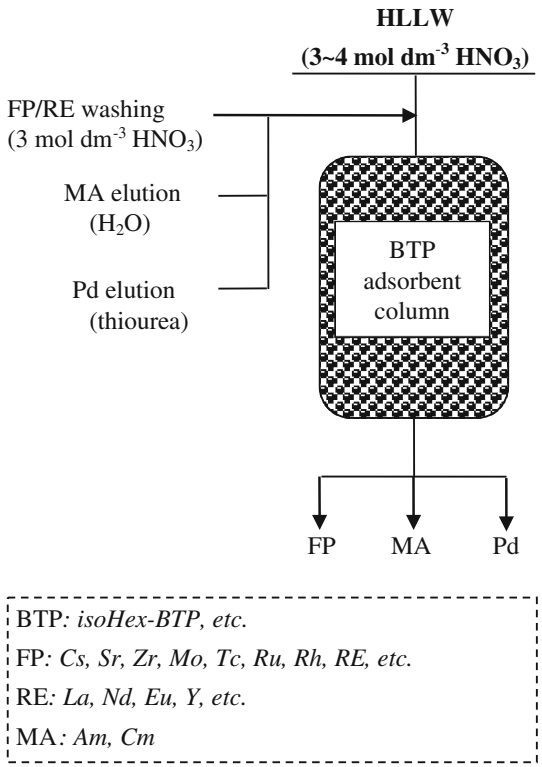

Fig. 1 Conceptual flowchart of the direct separation process of MA (III) from fission products (FP) present in HLLW by extraction chromatography

of the adsorbent). So the adsorbent may overcome the limitation of the low solubility of BTPs in traditional aliphatic diluents [23, 26]. Compared to liquid–liquid extraction method, the main advantages of the partitioning process include not only its high adsorption selectivity and affinity towards Am(III) over Ln(III) and other fission products present in HLLW, but also much smaller scale equipment than that of PUREX process, savings in reagent and waste disposal costs, possibility of direct separation of MA(III) in the column mode [24, 29, 30].

In the present work, to further study the properties of *iso*Hex-BTP/SiO_2-P, the adsorption behavior of ^{241}Am(III), ^{239}Pu(IV), ^{238}U(VI), Ln(III) and other typical fission products by *iso*Hex-BTP/SiO_2-P adsorbent from nitric acid solution was investigated. The effects of various parameters including contact time, initial concentration of Dy(III) and adsorption temperature on the adsorption of Dy(III) [as a simulated element of MA(III) and a representative element of Ln(III)] by *iso*Hex-BTP/SiO_2-P from 3 mol dm^{-3} nitric acid solution were studied. The experimental adsorption data depending on contact time were explained by the pseudo-first-order and pseudo-second-order kinetic models. The equilibrium adsorption data were analyzed using the Freundlich and Langmuir isotherm models. Thermodynamic parameters, Gibbs free energy change

(ΔG), enthalpy change (ΔH) and entropy change (ΔS), were calculated by using adsorption data changing on temperature to evaluate the thermodynamic feasibility and the spontaneous nature of the adsorption process.

Experimental

Materials and characterization

Various reagents, $RE(NO_3)_3{\cdot}nH_2O$ (RE: Y, La, Ce, Nd, Sm, Eu, Gd and Dy, $n = 5$ or 6), other fission product (FP) element nitrates [Sr(II) and Zr(IV)] and $(NH_4)_6Mo_7O_{24}{\cdot}4H_2O$, were of commercial reagents of analytical grade. The solutions of these metal ions were prepared by dissolving the reagents into nitric acid solutions. Ru(III) solution was obtained by diluting a commercially available nitrosyl nitrate solution containing 1.5 % of Ru(III). 1 mmol dm^{-3} of U(VI), trace amount of ^{241}Am(III), ^{152}Eu(III), ^{99}Tc(VII) and ^{239}Pu(IV) were prepared from their stocked solutions, respectively.

The purity of synthesized extracting agent, *iso*Hex-BTP, was 99 %. *iso*Hex-BTP/SiO_2-P adsorbent was prepared as described in the previous studies of Wei et al. [31–34] by impregnating *iso*Hex-BTP molecules into the pores of the silica/polymer composite support (SiO_2-P). *iso*Hex-BTP/SiO_2-P contained 0.5 g of *iso*Hex-BTP in 1.0 g of SiO_2-P, i.e. the content of extracting agent *iso*Hex-BTP was as high as 33.3 % of the total mass of the adsorbent. The chemical structure of *iso*Hex-BTP and scanning electron microscope (SEM) image of *iso*Hex-BTP/SiO_2-P are shown in Fig. 2 [29, 34].

Batch adsorption experiment

The adsorption behaviors of ^{241}Am(III) (1,000 Bq cm^{-3}), ^{239}Pu(IV) (50 Bq cm^{-3}), ^{238}U(VI) (1 mmol dm^{-3}), ^{152}Eu(III) (1,000 Bq cm^{-3}), ^{99}Tc(VII) (1,000 Bq cm^{-3}) and other typical fission products by *iso*Hex-BTP/SiO_2-P adsorbent from nitric acid medium were studied in a batch adsorption mode. The effects of adsorption parameters including contact time (10 min–72 h), initial Dy(III) concentration and adsorption temperature (288–308 K) on the adsorption of Dy(III) by *iso*Hex-BTP/SiO_2-P from 3 mol dm^{-3} nitric acid solution were studied in the batch adsorption mode, too.

For each batch experiment, 5 cm^3 of aqueous solution containing metal ions and nitric acid was added to 0.1 g *iso*Hex-BTP/SiO_2-P in a glass vial with Teflon stopper. The mixture was shaken mechanically at 120 rpm for predetermined contact time in a constant temperature water bath. Then the aqueous phase was filtrated through a membrane filter with 0.20 μm pore. The concentration of individual metal ions such as Sr(II), Y(III), Zr(IV), Mo(VI), Ru(III), La(III), Ce(III), Nd(III), Sm(III), Eu(III), Gd(III) and Dy(III) present in aqueous phase before and after the adsorption was analyzed by Inductively Coupled Plasma Atomic Emission Spectroscopy (ICP-AES: Shimadzu ICPS-7510). The individual radioactivity of ^{241}Am and ^{152}Eu was determined by HPGe-γ-detector (GEM70P-PLUS, Ortec). The individual radioactivity of ^{99}Tc(VII) and ^{239}Pu(IV) was measured by Super Low Level Liquid Scintillation Analyzer (PE Tri-Carb 3170). The concentration of U(VI) was measured by UV spectrophotometer (LabTech UV1000/1100).

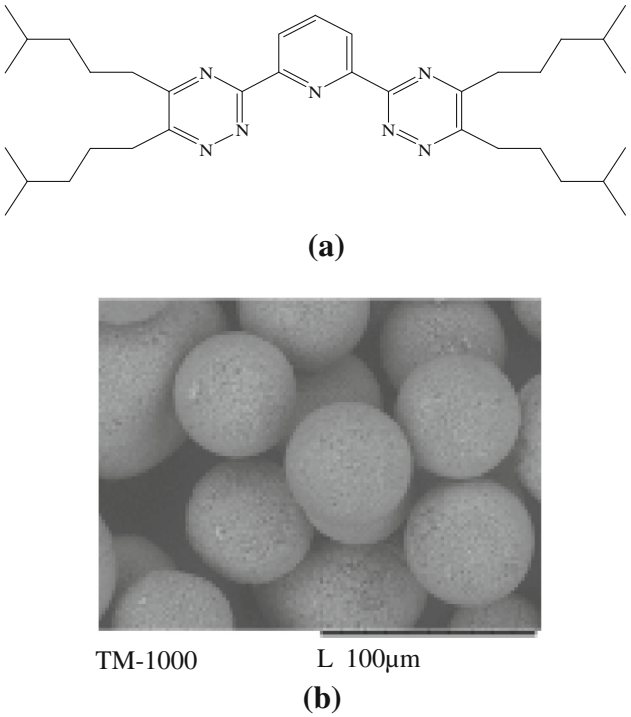

Fig. 2 Chemical structure of *iso*Hex-BTP (**a**) and SEM image of *iso*Hex-BTP/SiO_2-P (**b**)

In a batch experiment, the distribution coefficient (K_d, cm^3 g^{-1}) was calculated by Eq. (1) or Eq. (2):

$$K_d(\mathrm{cm^3\ g^{-1}}) = \frac{C_0 - C_e}{C_e} \cdot \frac{V}{W_R} \quad (1)$$

$$K_d(\mathrm{cm^3\ g^{-1}}) = \frac{A_0 - A_e}{A_e} \cdot \frac{V}{W_R} \quad (2)$$

The equilibrium adsorption capacity, q_e (mmol g^{-1}), and the adsorption capacity at the time t, q_t (mmol g^{-1}), were obtained using Eqs. (3) and (4), respectively:

$$q_e(\mathrm{mmol\ g^{-1}}) = \frac{(C_0 - C_e)\ V}{1{,}000 \times W_R} \quad (3)$$

$$q_t(\text{mmol g}^{-1}) = \frac{(C_0 - C_t)\ V}{1{,}000 \times W_R} \quad (4)$$

where C_0 (mmol dm^{-3}) [A_0 (Bq cm^{-3})] and C_e (mmol dm^{-3}) [A_e (Bq cm^{-3})] are the concentration (radioactivity) of metal ions in the aqueous phase initially and at equilibrium, respectively. V (cm^3) and W_R (g) indicate the volume of the aqueous phase and the weight of *iso*Hex-BTP/SiO_2-P, respectively. C_t (mmol dm^{-3}) is the metal ion concentration in aqueous phase at a given contact time t.

Most of the experiments were repeated three times for better accuracy and blank experiments were also performed in this study. The experimental error was observed to be within ±5 %.

Experimental results

Selective adsorption of Am(III) and Pu(IV) by isoHex-BTP/SiO_2-P

To study the impact of the initial nitric acid concentration on the adsorption of actinides and some typical fission products by *iso*Hex-BTP/SiO_2-P, 0.1 g *iso*Hex-BTP/SiO_2-P was batch equilibrated with 5 cm^3 of solution containing ^{241}Am(III) (1,000 Bq cm^{-3}), ^{152}Eu(III) (1,000 Bq cm^{-3}), ^{99}Tc(VII) (1,000 Bq cm^{-3}), ^{239}Pu(IV) (50 Bq cm^{-3}), 1 mmol dm^{-3} ^{238}U(VI) and stable Eu(III) at various initial nitric acid concentrations for 24 h of contact. Figure 3 shows the plots of distribution coefficients, K_d, of these nuclides with varying nitric acid concentration. Evidently, K_d of

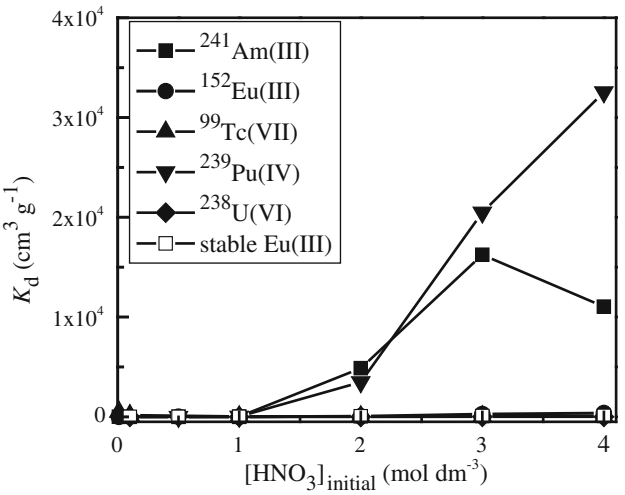

Fig. 3 Effect of initial nitric acid concentration on the distribution coefficient of ^{241}Am(III), ^{152}Eu(III), ^{239}Pu(IV), ^{99}Tc(VII), ^{238}U(VI) and stable Eu(III) (298 K, phase ratio: 0.1 g 5 cm^{-3}, trace amount of ^{241}Am(III), ^{152}Eu(III), ^{99}Tc(VII) and ^{239}Pu(IV), ^{238}U(VI) and stable Eu(III): 1 mmol dm^{-3}, shaking speed: 120 rpm, contact time: 24 h)

Table 1 Distribution coefficients of trace amount of ^{152}Eu(III) and 1 mmol dm^{-3} stable Eu(III) (298 K, phase ratio: 0.1 g 5 cm^{-3}, shaking speed: 120 rpm, contact time: 24 h)

	$[HNO_3]_{initial}$ (mol dm^{-3})					
	0.01	0.5	1	2	3	4
$K_{d\ ^{152}Eu(III)}$ (cm^3 g^{-1})	0	0	0	55	266	369
$K_{d\ stable\ Eu(III)}$ (cm^3 g^{-1})	0	0	0	55	78	88

Am(III) remarkably increased from 1 to 16,200 cm^3 g^{-1} with increasing nitric acid concentration from 0.01 to 3 mol dm^{-3} owing to the participation of NO_3^- in complexation reaction between Am(III) and *iso*Hex-BTP/SiO_2-P [29]. And then the slight decrease of K_d of Am(III) from 3 mol dm^{-3} to higher concentration of nitric acid is thought to be due to a competition reaction of Am(III) or HNO_3 with *iso*Hex-BTP/SiO_2-P [17]. While for Pu(IV), K_d extraordinarily increased from 3 to 34,500 cm^3 g^{-1} with increasing nitric acid concentration from 0.5 to 4 mol dm^{-3}. Generally, both Am(III) and Pu(IV) were adsorbed efficiently from 2 to 4 mol dm^{-3} nitric acid solutions. However, the adsorption of ^{152}Eu(III), ^{99}Tc(VII) and U(VI) was very weak throughout the investigated nitric acid concentration range (0.01–4 mol dm^{-3}). Although the distribution coefficients of trace amount of ^{152}Eu(III) were higher than those of 1 mmol dm^{-3} stable Eu(III) in 2–4 mol dm^{-3} nitric acid solutions as shown in Fig. 3 and Table 1, they are still much lower than those of trace amount of Pu(IV) and Am(III). The order of adsorbability was Pu(IV) > Am(III) ≫ Eu(III), Tc(VII) and U(VI) within the nitric acid concentration range of 2–4 mol dm^{-3}.

Since *iso*Hex-BTP/SiO_2-P is a potential adsorbent in the direct separation process of MA (III) from HLLW by extraction chromatography in our research work, knowing its selectivity for Am(III) and Pu(IV) over Eu(III), U(VI) and Tc(VII) does not suffice. According to the nitric acid concentration of HLLW (about 3 mol dm^{-3}) and the experimental data in Fig. 3, 3 mol dm^{-3} HNO_3 solution was chosen to investigate the adsorption of actinides [i.e. ^{241}Am(III), ^{239}Pu(IV) and ^{238}U(VI)] and some typical fission products by *iso*Hex-BTP/SiO_2-P for 24 h of contact at 298 K. The distribution coefficient of each element is illustrated in Fig. 4. It can be observed that Sr(II), Zr(IV), Mo(VI), Tc(VII), Ru(III), Y(III), all Ln(III) and U(VI) showed very weak or almost no adsorption towards *iso*-Hex-BTP/SiO_2-P. Such low values in the distribution coefficient were due to the weak complexation of these metal ions with *iso*Hex-BTP/SiO_2-P. Contrastively, K_d values of Pu(IV) (20,400 cm^3 g^{-1}) and Am(III) (16,200 cm^3 g^{-1}) were extremely high. The reason is that the radial extension of the 5*f* orbitals of Pu(IV) and Am(III) is further than the 4*f* orbitals of Ln(III) and outermost

electron orbitals of other fission products, which causes bonds of Pu(IV) and Am(III) to have more covalent character and Pu(IV) and Am(III) forming more stable complexes with *iso*Hex-BTP/SiO_2-P [35]. The extremely high selectivity of Pu(IV) can be interpreted as the size fit of *iso*Hex-BTP cavity being preferable for Pu(IV), which needs further researches [7, 17, 35]. The separation factors between ^{241}Am(III) or ^{239}Pu(IV) and the most affinity nuclide, Eu(III), among the other experimental metal ions, $SF_{^{241}Am/^{152}Eu}$ ($SF_{^{241}Am/^{152}Eu} = K_{d\,^{241}Am}/K_{d^{152}Eu}$) and $SF_{^{239}Pu/^{152}Eu}$($SF_{^{239}Pu/^{152}Eu} = K_{d\,^{239}Pu}/K_{d^{152}Eu}$), were 61 and 77, respectively. The separation factors between ^{241}Am(III) or ^{239}Pu(IV) and the other metal ions were far more than 100.

As described in our previous report [29], *iso*Hex-BTP/SiO_2-P exhibited high selectivity for Am(III) over Ln(III) and other typical fission products. These results in the present work further suggest that *iso*Hex-BTP/SiO_2-P has relatively high selectivity and affinity for Am(III) and Pu(IV) over U(VI), Tc(VII), Eu(III) and other typical fission products in 3 mol dm^{-3} nitric acid solution. And the adsorbed Am(III) and Pu(IV) can be stripped into dilute nitric acid (<0.1 mol dm^{-3}) or distilled water because Am(III) and Pu(IV) showed almost no adsorption in ≤1 mol dm^{-3} nitric acid solutions and the adsorption of Am(III) and Pu(IV) is readily reversible by changing the nitric acid concentration (as shown in Fig. 3). So it is possible to direct separate Am(III) and residual Pu(IV) from other metal ions present in HLLW by extraction chromatography using *iso*Hex-BTP/SiO_2-P.

According to Fig. 4 and our previous work [29, 30], K_d value of Dy(III) was dominantly higher than those of other fission products in 3 mol dm^{-3} HNO_3 and the adsorption behavior of Dy(III) by BTP/SiO_2-P adsorbent was similar to that of MA(III) owing to their similar coordination chemistry [6, 7]. Furthermore, Dy(III) is hardly contained in HLLW. So as a simulated element of MA(III) and a representative element of Ln(III), Dy(III) adsorption by *iso*Hex-BTP/SiO_2-P from 3 mol dm^{-3} nitric acid solution was investigated to evaluate its adsorption kinetics, isotherms and thermodynamics in this study.

Effect of contact time on Dy(III) adsorption

To determine the equilibrium time for the adsorption, Dy(III) (initial concentration: 6 mmol dm^{-3}) adsorption by *iso*Hex-BTP/SiO_2-P from 3 mol dm^{-3} HNO_3 solution was studied as a function of contact time at different temperatures (288, 298 and 308 K, respectively). The results are shown in Fig. 5. Generally, Dy(III) adsorption capacity increased with the increase in contact time and temperature. With increasing contact time, a rapid initial Dy(III) adsorption within the first 3 h of contact was followed by a steady stage which finally reached an apparent plateau until adsorption equilibrium was attained. 48.8, 79.6 and 88.4 % of the equilibrium adsorption capacity of Dy(III) occurred within the first 3 h at 288, 298 and 308 K, respectively. The sudden increase of q_t at the very beginning of the process is attributed to an abundant availability of active sites on internal and external surface area of *iso*Hex-BTP/SiO_2-P. With the progressive occupancy of these sites by Dy(III), the process comes into a period of slower adsorption, during which the less accessible sites can be occupied by Dy(III). Furthermore, the experimental equilibrium adsorption capacity ($q_{e,exp}$) of Dy(III) increased from 0.14 to 0.17 mmol g^{-1} when adsorption temperature increased from 288 to 308 K (as shown in Fig. 5 and Table 2).

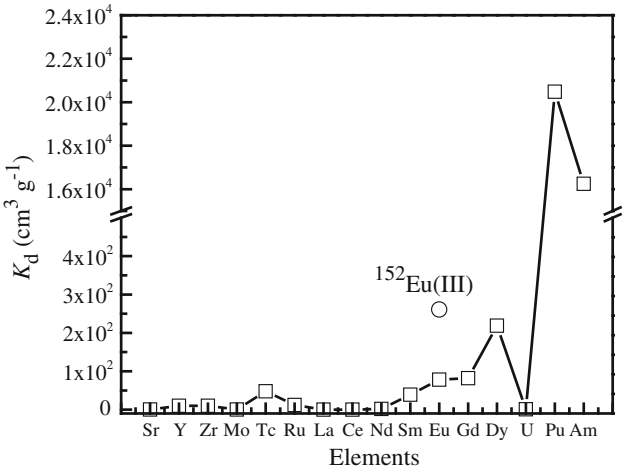

Fig. 4 Adsorption of actinides, lanthanides (III) and other typical fission products by *iso*Hex-BTP/SiO_2-P (298 K, $[HNO_3]_{initial}$: 3 mol dm^{-3}, phase ratio: 0.1 g 5 cm^{-3}, trace amount of ^{241}Am(III), ^{239}Pu(IV), ^{99}Tc(VII) and ^{152}Eu(III), stable Eu(III) and other metal ion concentration: 1 mmol dm^{-3}, shaking speed: 120 rpm, contact time: 24 h)

Effect of initial Dy(III) concentration on adsorption capacity

The equilibrium adsorption capacity of Dy(III) by *iso*Hex-BTP/SiO_2-P is a function of both the initial Dy(III) concentration and the adsorption temperature. The effect of initial Dy(III) concentration ranging from 2 to 6 mmol dm^{-3} on the equilibrium adsorption capacity of Dy(III) for constant contact time (t = 72 h, to obtain the complete equilibrium state) at constant temperature (288, 298 and 308 K, respectively) is plotted in Fig. 6. Apparently, the equilibrium adsorption capacity of Dy(III) (q_e) increased by increasing the initial concentration of Dy(III) and then reached the

maximum adsorption capacity (q_m) at high initial concentration. It was observed that at lower initial concentration of Dy(III), the equilibrium adsorption capacity increased with increasing the temperature from 288 to 308 K due to higher utilization of active sites of *iso*Hex-BTP/SiO_2-P at higher temperatures. However, the experimental maximum adsorption capacity, $q_{m,exp}$, almost remained constant ($q_{m,exp} = 0.16$, 0.17 and 0.17 mmol g^{-1} at 288, 298 and 308 K, respectively, as shown in Fig. 6 and Table 3) despite of increasing temperature because the total existing adsorption sites of *iso*Hex-BTP/SiO_2-P are confined, which resulted in a saturation adsorption of Dy(III) [36, 37].

Discussion

Adsorption kinetics

In order to examine the mechanism of adsorption potential rate controlling steps such as mass-transport, and chemical reaction processes of the adsorption of Dy(III) by *iso*Hex-BTP/SiO_2-P, the experimental data obtained in the "Effect of contact time on Dy(III) adsorption" were further analyzed using the pseudo-first-order and pseudo-second-order kinetic models.

The pseudo-first-order kinetic model is based on the approximation that the adsorption rate relates to the number of the unoccupied, adsorptive sites [38]. The linear form of the model can be expressed as Eq. (5) [38, 39]:

$$\ln(q_e - q_t) = \ln q_e - k_1 t \quad (5)$$

where q_e (mmol g^{-1}) and q_t (mmol g^{-1}) are the adsorption capacity at equilibrium and at any time t (h), and k_1 is the adsorption rate constant (h^{-1}).

The value of the adsorption rate constant (k_1) can be calculated by plotting of $\ln(q_e - q_t)$ versus t. k_1 and the correlation coefficients (R^2) at various temperatures were determined as summarized in Table 2. R^2 was fairly low ($R^2 = 0.983$, 0.670 and 0.531 at 288, 298 and 308 K, respectively) and the value of k_1 decreased from 0.11 to 0.08 h^{-1} with increase in temperature from 288 to 308 K

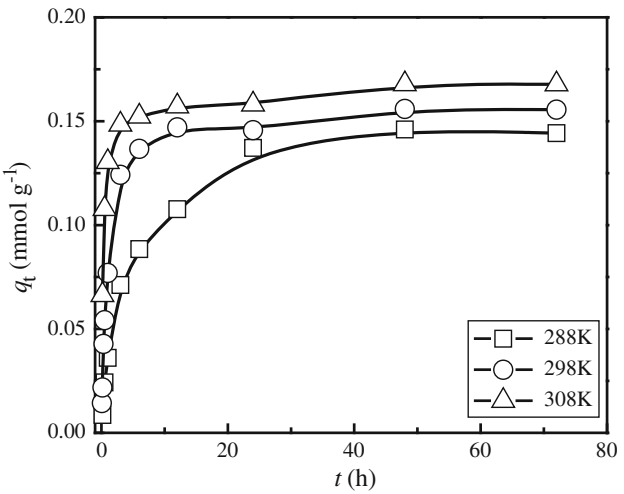

Fig. 5 Effect of contact time on adsorption capacity of Dy(III) by *iso*Hex-BTP/SiO_2-P at various temperatures ($[HNO_3]_{initial}$: 3 mol dm^{-3}, $[Dy(III)]_{initial}$: 6 mmol dm^{-3}, phase ratio: 0.1 g 5 cm^{-3}, shaking speed: 120 rpm)

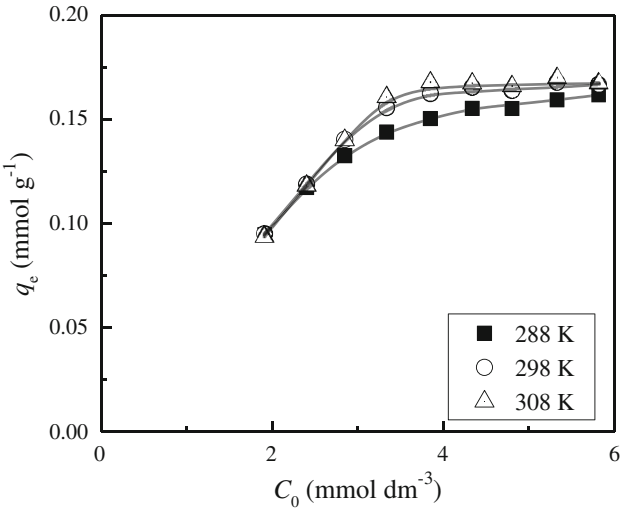

Fig. 6 Effect of initial Dy(III) concentration ranging from 2 to 6 mmol dm^{-3} on the equilibrium adsorption capacity of Dy(III) by *iso*Hex-BTP/SiO_2-P at different temperatures (phase ratio: 0.1 g 5 cm^{-3}, shaking speed: 120 rpm, contact time: 72 h)

Table 2 The adsorption kinetic model parameters for Dy(III) adsorption by *iso*Hex-BTP/SiO_2-P at various temperatures ($[HNO_3]_{initial}$: 3 mol dm^{-3}, $[Dy(III)]_{initial}$: 6 mmol dm^{-3}, phase ratio: 0.1 g 5 cm^{-3}, shaking speed: 120 rpm)

T (K)	Pseudo-first-order kinetic model		Pseudo-second-order kinetic model				Experimental $q_{e,exp}$ (mmol g^{-1})
	k_1 (h^{-1})	R^2	$q_{e,calc}$ (mmol g^{-1})	k_2 (g mmol^{-1} h^{-1})	h (mmol g^{-1} h^{-1})	R^2	
288	0.11	0.983	0.15	1.99	0.05	0.988	0.14
298	0.12	0.670	0.15	8.05	0.19	0.999	0.16
308	0.08	0.531	0.16	26.29	0.67	1.000	0.17

which conflicted with the experimental phenomenon, indicating that the adsorption process does not fit to the pseudo-first-order kinetic model.

Experimental data were also applied to the pseudo-second-order kinetic model which is based on the assumption that chemisorption is the rate-determining step of adsorption process [40]. The linear form of the model can be expressed as Eq. (6) [39, 40]:

$$\frac{t}{q_t} = \frac{1}{k_2 q_e^2} + \frac{t}{q_e} \quad (6)$$

where q_t (mmol g^{-1}) and q_e (mmol g^{-1}) are the adsorption capacity at any time t and at equilibrium, k_2 (g $mmol^{-1}$ h^{-1}) is the adsorption rate constant of pseudo-second-order kinetic model.

The adsorption rate constant k_2 and the calculated equilibrium capacity $q_{e,calc}$ can be calculated by plotting of t/q_t versus t for Dy(III) adsorption by *iso*Hex-BTP/SiO_2-P. The kinetic parameters including k_2, $q_{e,calc}$, h (initial adsorption rate, $h = k_2 q_e^2$) and R^2 (correlation coefficient) at various temperatures are listed in Table 2. As shown in Table 2, R^2 for the pseudo-second-order kinetic plot increased from 0.988 to 1.000 with increasing temperature from 288 to 308 K and $q_{e,calc}$ was almost equal to the experimental one ($q_{e,exp}$) at each temperature. The results indicate that Dy(III) adsorption by *iso*Hex-BTP/SiO_2-P fits much better to the pseudo-second-order kinetic model than the pseudo-first-order kinetic model. Therefore, it could be concluded that the adsorption is of the chemisorption type due to sharing of electrons between *iso*-Hex-BTP and *4f* orbital of Dy(III) and the coordination reaction between *iso*Hex-BTP and Dy(III) is the rate-controlling step of the kinetic behavior of adsorption [7, 17, 39]. Furthermore, the goodness of fitting of Dy(III) adsorption is more favorable at higher temperature. $q_{e,exp}$ and $q_{e,calc}$ increased from 0.14 to 0.17 mmol g^{-1} and from 0.15 to 0.16 mmol g^{-1}, respectively, with increasing the temperature from 288 to 308 K. Presumably the increase in adsorption capacity may be attribute to the strengthening of adsorptive forces between the active sites of *iso*Hex-BTP/SiO_2-P and Dy(III) at higher temperatures. Meanwhile, k_2 and h increased dramatically from 1.99 to 26.29 g $mmol^{-1}$ h^{-1} and from 0.05 to 0.67 mmol g^{-1} h^{-1}, respectively, by raising temperature. The increase in adsorption rate is correlated to the acceleration in complexation reaction between Dy(III) and *iso*Hex-BTP/SiO_2-P as the rate-controlling step of adsorption and acceleration of some originally slow steps such as diffusion of Dy(III) in solution at higher temperatures.

In view of the adsorption temperature of 288 K, the adsorption kinetic data fit well to both the pseudo-first-order and pseudo-second-order kinetic models with relatively high correlation coefficients ($R^2 = 0.983$ and 0.988, respectively). One may be tempted to argue that the Dy(III) adsorption by *iso*Hex-BTP/SiO_2-P at lower temperatures is more correctly described by more than one adsorption kinetic models.

Adsorption isotherms

Adsorption isotherms describe the relationship between the equilibrium concentration of metal ions in solution and the amount of metal ions adsorbed on a specific adsorbent at a constant temperature. The adsorption isotherms of Dy(III) by *iso*Hex-BTP/SiO_2-P as shown in Fig. 7 were obtained from the experimental data in "Effect of initial Dy(III) concentration on adsorption capacity" section. As shown in Fig. 7, the adsorption capacity of Dy(III) increased as the equilibrium concentration of Dy(III) increased, then reached a steady stage which finally reached the maximum adsorption capacity. The equilibrium concentration C_e of Dy(III) in solution decreased with increasing temperature, i.e. the adsorption is favored at higher temperatures.

The equilibrium data for Dy(III) adsorption were also analyzed with the most common adsorption isotherm models, the Freundlich and Langmuir isotherm models, to reveal the adsorption mechanism [38, 41].

The Freundlich adsorption isotherm model is used to describe the adsorption of an adsorbate on a heterogeneous surface of an adsorbent. The linear form of the model is given as Eq. (7) [38]:

$$\log q_e = \log K_F + \frac{1}{n_F} \log C_e \quad (7)$$

where K_F is a constant related to the maximum adsorption capacity and $1/n_F$ is an empirical parameter related to the adsorption intensity.

Linear plot of $\log q_e$ versus $\log C_e$ shows that the adsorption follows the Freundlich isotherm model. K_F and n_F were calculated from the intercept and the slope of the plot. The parameters n_F, K_F and R^2 (correlation coefficient) for Dy(III) and *iso*Hex-BTP/SiO_2-P system at various temperatures of 288, 298 and 308 K in the Freundlich equation are summarized in Table 3.

The Langmuir adsorption isotherm model is widely used to describe the adsorption of an adsorbate on a homogeneous, flat surface of an adsorbent and each adsorptive site can be occupied only once in a one-on-one manner [38]. Mathematically, the linear form of the model is given in Eq. (8) [39]:

$$\frac{C_e}{q_e} = \frac{1}{K_L q_m} + \frac{C_e}{q_m} \quad (8)$$

where q_e (mmol g^{-1}) is the adsorption capacity at equilibrium, C_e (mmol dm^{-3}) is the equilibrium concentration of an adsorbate in solution, q_m (mmol g^{-1}) is the maximum adsorption capacity to form a monolayer onto an adsorbent surface, K_L (dm^3 $mmol^{-1}$) is Langmuir adsorption constant related to energy of adsorption which quantitatively reflects

Table 3 The Freundlich and Langmiur adsorption isotherm parameters and their correlation coefficients at various temperatures ($[HNO_3]_{initial}$: 3 mol dm^{-3}, phase ratio: 0.1 g 5 cm^{-3}, shaking speed: 120 rpm, contact time: 72 h)

T (K)	Freundlich isotherm parameters			Langmiur isotherm parameters				Experimental $q_{m,exp}$ (mmol g^{-1})
	n_F	K_F (mmol g^{-1})	R^2	$q_{m,calc}$ (mmol g^{-1})	K_L (dm^3 $mmol^{-1}$)	R_L	R^2	
288	8.67	0.16	0.953	0.16	23.44	0.022–0.007	0.999	0.16
298	9.12	0.17	0.794	0.17	74.25	0.007–0.002	1.000	0.17
308	11.12	0.18	0.621	0.17	105.64	0.005–0.002	1.000	0.17

that affinity between the adsorbent and adsorbate. The fundamental characteristic of a Langmuir isotherm parameter (R_L) can be expressed in terms of a dimensionless separation factor or an equilibrium parameter, which is defined by Eq. (9) [38]:

$$R_L = \frac{1}{1 + K_L C_0} \tag{9}$$

where C_0 (mmol dm^{-3}) is the initial concentration of an adsorbate. According to the value of R_L, the shape of the isotherm may be interpreted as follows: $R_L > 1$: unfavorable adsorption, $R_L = 1$: linear adsorption, $0 < R_L < 1$: favorable adsorption, $R_L = 0$: irreversible adsorption [38].

The linear plot of C_e/q_e versus C_e shows that the adsorption of Dy(III) by *iso*Hex-BTP/SiO_2-P obeys Langmuir isotherm model. The values of q_m and K_L were determined from the slope ($1/q_m$) and intercept ($1/K_L q_m$) of the Langmuir plot. Langmuir parameters for fitting adsorption data, $q_{m,calc}$ (the calculated maximum adsorption capacity), K_L, R_L and R^2 (the correlation coefficient) values at various temperatures are reported in Table 3.

As can be seen, the correlation coefficient ($R^2 \geq 0.999$) for the Langmuir isotherm plot was much higher than that for the Freundlich plot ($0.621 \leq R^2 \leq 0.953$) at individual temperature. The calculated maximum adsorption capacity ($q_{m,calc} = 0.16$, 0.17 and 0.17 mmol g^{-1} at 288, 298 and 308 K, respectively) from Langmuir isotherm model was equal to the experimental one $q_{m,exp}$ at each individual temperature. The results indicate that the equilibrium adsorption data fit much better to the Langmuir isotherm model than the Freundlich isotherm model, which means that adsorption of Dy(III) occurs on a homogeneous surface by monolayer sorption and each adsorptive site of *iso*Hex-BTP/SiO_2-P can be occupied by Dy(III) only once in a one-on-one manner. Both $q_{m,calc}$ and $q_{m,exp}$ slightly increased from 0.16 to 0.17 mmol g^{-1}, with increasing the solution temperature. The increase in maximum adsorption capacity may be due to the higher coordination reaction between Dy(III) and *iso*Hex-BTP/SiO_2-P and the higher utilization of all available active sites of *iso*Hex-BTP/SiO_2-P for adsorption at higher temperatures. However, the increase in the maximum adsorption capacity with increasing the temperature from 288 to 308 K was very limited (as shown in Table 3). The reasonable conjecture is a saturation adsorption of Dy(III) towards the total existing adsorption sites on internal and external surface area of *iso*Hex-BTP/SiO_2-P to form a monolayer adsorption, as discussed in "Effect of initial Dy(III) concentration on adsorption capacity" section. High K_L values indicate high adsorption affinity. K_L values dramatically increased from 23.44 to 105.64 dm^3 $mmol^{-1}$ with increasing the temperature from 288 to 308 K, suggesting that increasing temperature could increase the affinity of *iso*Hex-BTP/SiO_2-P for Dy(III). The values of R_L ($0 < R_L < 1$) indicate that the adsorption of Dy(III) by *iso*Hex-BTP/SiO_2-P is favorable. Furthermore, R_L values decreased with increasing temperature, revealing that the adsorption reaction is more favorable at higher temperature than lower temperature.

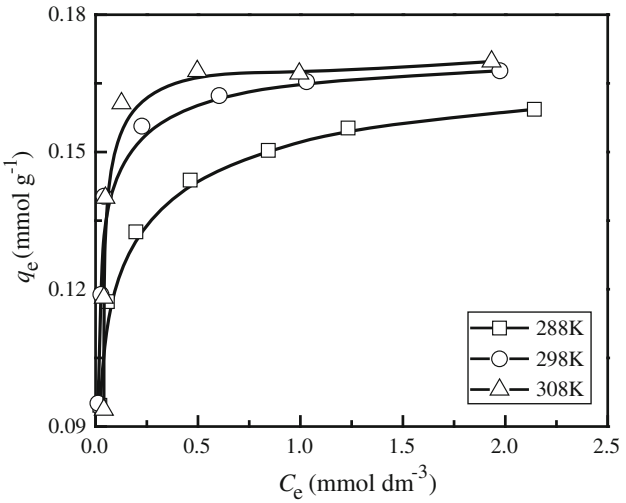

Fig. 7 Adsorption isotherms of Dy(III) by *iso*Hex-BTP/SiO_2-P at various temperatures ($[HNO_3]_{initial}$: 3 mol dm^{-3}, phase ratio: 0.1 g 5 cm^{-3}, shaking speed: 120 rpm, contact time: 72 h)

Adsorption thermodynamics

From the adsorption kinetics and isotherm results, it can be seen that the increase in temperature generally increased the adsorption properties of Dy(III) by *iso*Hex-BTP/SiO_2-

Table 4 Adsorption thermodynamic parameters for Dy(III) adsorption by *iso*Hex-BTP/SiO_2-P ($[HNO_3]_{initial}$: 3 mol dm^{-3}, $[Dy(III)]_{initial}$: 6 mmol dm^{-3}, phase ratio: 0.1 g 5 cm^{-3}, shaking speed: 120 rpm, contact time: 48 h)

ΔH (kJ mol^{-1})	ΔS (kJ mol^{-1} K^{-1})	ΔG(kJ mol^{-1})			R^2
		288 K	298 K	308 K	
7.25	0.06	−10.03	−10.63	−11.23	0.911

P. So values of thermodynamic parameters including enthalpy change (ΔH), entropy change (ΔS) and Gibbs free energy change (ΔG) were determined to confirm the adsorption nature.

In order to obtain the thermodynamic parameters, the temperature dependence of Dy(III) adsorption by *iso*Hex-BTP/SiO_2-P at equilibrium was examined at initial Dy(III) concentration of 6 mmol dm^{-3} in the temperature range from 288 to 308 K. Thermodynamic parameters, ΔH, ΔS and ΔG, associated to the adsorption process were determined using Eqs. (10) and (11) [39, 41]:

$$\ln K_d = \frac{\Delta S}{R} - \frac{\Delta H}{RT} \quad (10)$$

$$\Delta G = \Delta H - T\Delta S \quad (11)$$

where K_d, ΔS, ΔH, ΔG, T and R are the distribution coefficient, the entropy change (kJ mol^{-1} K^{-1}), the enthalpy change (kJ mol^{-1}), Gibbs free energy change (kJ mol^{-1}), absolute temperature (K) and the universal gas constant (0.0083 kJ mol^{-1} K^{-1}), respectively.

ΔH and ΔS for the adsorption of Dy(III) by *iso*Hex-BTP/SiO_2-P can be individually derived from the slope and intercept of the plot of $\ln K_d$ versus $1/T$ from Eq. (10). The thermodynamic parameters are summarized in Table 4. Obviously, the negative ΔG value in each individual temperature indicates that the adsorption of Dy(III) by *iso*Hex-BTP/SiO_2-P is thermodynamically feasible and spontaneous and the adsorption process would be a product-favored reaction [42]. The ΔG values became more negative with the rise in temperature suggesting that spontaneous nature of adsorption increases at higher temperatures. The positive value of enthalpy change ($\Delta H = 7.25$ kJ mol^{-1}) verifies the endothermic nature of the Dy(III) adsorption by *iso*Hex-BTP/SiO_2-P. The positive value of ΔS suggests the increase in the degree of randomness at the solid-solution interface mostly encountered in Dy(III) binding due to the release of water molecules of the hydration sphere [42] during the fixation of Dy(III) on *iso*Hex-BTP/SiO_2-P surface [38]. Furthermore, the positive ΔS value, 0.06 kJ mol^{-1} K^{-1}, indicates that the adsorption process is probably irreversible and favored complexation and stability of adsorption [39]. Although the enthalpy change value was positive, Gibbs free energy change was negative at each individual temperature and the adsorption was spontaneous, which indicates that Dy(III) adsorption by *iso*Hex-BTP/SiO_2-P is an entropy-driving process.

Conclusions

Within the scope of this work, the *iso*Hex-BTP/SiO_2-P adsorbent exhibited remarkable selectivity and affinity for Am(III) and Pu(IV) over U(VI), Eu(III), Tc(VII) and other typical fission products in 3 mol dm^{-3} nitric acid solution. Many factors such as contact time, initial concentration of Dy(III) and adsorption temperature had strong impacts on adsorption of Dy(III) (as a simulated element of MA(III) and a representative element of Ln(III)) by *iso*Hex-BTP/SiO_2-P from 3 mol dm^{-3} nitric acid solution. The adsorption data depending on contact time fit much better to the pseudo-second-order kinetic model with high correlation coefficients ($0.988 \leq R^2 \leq 1.000$) than the pseudo-first-order kinetic model, indicating that Dy(III) adsorption by *iso*Hex-BTP/SiO_2-P occurs by chemisorption mechanism and the coordination reaction between *iso*Hex-BTP and Dy(III) is the rate-controlling step of the adsorption process. The adsorption data depending on initial Dy(III) concentration were analyzed by the Freundlich and Langmuir isotherm models. The equilibrium adsorption data follow much better the Langmuir isotherm model than the Freundlich isotherm model at the each individual temperature of 288, 298 and 308 K, which means that the adsorption of Dy(III) occurs on a homogeneous surface of *iso*Hex-BTP/SiO_2-P and each adsorptive site of *iso*Hex-BTP/SiO_2-P can be occupied by Dy(III) only once in a one-on-one manner. The values of Gibbs free energy change ($\Delta G = -10.03$, -10.63 and -11.23 kJ mol^{-1} at 288, 298 and 308 K, respectively), enthalpy change ($\Delta H = 7.25$ kJ mol^{-1}) and entropy change ($\Delta S = 0.06$ kJ mol^{-1} K^{-1}) indicate that the adsorption process is spontaneous, the endothermic nature and an entropy-driving process. These results also revealed that increasing temperature is benefit to the adsorption process of Dy(III) towards *iso*Hex-BTP/SiO_2-P by increasing the equilibrium adsorption capacity, the maximum adsorption capacity, the adsorption rate, the adsorption affinity and the spontaneous nature of adsorption process.

The results demonstrated that *iso*Hex-BTP/SiO_2-P is a promising adsorbent for the direct separation of Am(III) and residual Pu(IV) from Ln(III) and other typical elements

present in HLLW. Through this study, essential adsorption kinetics, adsorption isotherm and thermodynamics data were collected for an engineering design of the column separation of MA(III) from HLLW by *iso*Hex-BTP/SiO_2-P. In addition, more detailed property evaluations of *iso*Hex-BTP/SiO_2-P by column separation experiments are under the way.

Acknowledgments This work was supported by National Natural Science Foundation of China (Grant No. 11305102, 91126006, 21261140335, 91226111) and Doctoral Fund of Ministry of Education of China (Grant No. 20130073110046).

References

1. Madic C, Boullis B, Baron P, Testard R, Hudson MJ, Lijenzin JO, Christiansen B, Ferrando M, Facchini A, Geist A, Modolo G, Espartero AG, De Mendoza J (2007) Futuristic back-end of the nuclear fuel cycle with the partitioning of minor actinides. J Alloys Compd 444:23–27
2. Madic C, Hudson MJ, Liljenzin JO, Glatz JP, Nannicini R, Facchini A, Kolarik Z, Odoj R (2002) Recent achievements in the development of partitioning processes of minor actinides from nuclear wastes obtained in the frame of the NEWPART European programme (1996–1999). Prog Nucl Energy 40:523–526
3. Malmbeck R, Courson O, Pagliosa G, Romer K, Satmark B, Glatz JP, Baron P (2000) Partitioning of minor actinides from HLLW using the DIAMEX process. Part 2—"Hot" continuous counter-current experiment. Radiochim Acta 88:865–871
4. Salvatores M, Palmiotti G (2011) Radioactive waste partitioning and transmutation within advanced fuel cycles: achievements and challenges. Prog Part Nucl Phys 66:144–166
5. Trumm S, Geist A, Panak PJ, Fanghanel T (2011) An improved hydrolytically-stable Bis-Triazinyl-Pyridine (BTP) for selective actinide extraction. Solvent Extr Ion Exch 29:213–229
6. Geist A, Hill C, Modolo G, Foreman M, Weigl M, Gompper K, Hudson MJ (2006) 6,6′-bis (5,5,8,8-tetramethyl-5,6,7,8-tetrahydro-benzo [1, 2, 4] triazin-3-yl) [2,2′] bipyridine, an effective extracting agent for the separation of americium(III) and curium(III) from the lanthanides. Solvent Extr Ion Exch 24:463–483
7. Denecke MA, Rossberg A, Panak PJ, Weigl M, Schimmelpfennig B, Geist A (2005) Characterization and comparison of Cm(III) and Eu(III) complexed with 2,6-di(5,6-dipropyl-1,2,4-triazin-3-yl)pyridine using EXAFS, TRFLS, and quantum-chemical methods. Inorg Chem 44:8418–8425
8. Mathur JN, Murali MS, Ruikar PB, Nagar MS, Sipahimalani AT, Bauri AK, Banerji A (1998) Degradation, cleanup, and reusability of octylphenyl-N, N′-diisobutylcarbamoylmethyl phosphine oxide (CMPO) during partitioning of minor actinides from high level waste (HLW) solutions. Sep Sci Technol 33:2179–2196
9. Patil AB, Shinde VS, Pathak PN, Mohapatra PK, Manchanda VK (2013) Modified synthesis scheme for N, N′-dimethyl-N, N′-dioctyl-2, (2′-chexyloxyethyl) malonamide (DMDOHEMA) and its comparison with proposed solvents for actinide partitioning. Radiochim Acta 101:93–100
10. Chen J, Wang JC (2011) Overview of 30 years research on TRPO process for actinides partitioning from high level liquid waste. Prog Chem 23:1366–1371
11. Paiva AP, Malik P (2004) Recent advances on the chemistry of solvent extraction applied to the reprocessing of spent nuclear fuels and radioactive wastes. J Radioanal Nucl Chem 261:485–496
12. Ansari SA, Pathak P, Mohapatra PK, Manchanda VK (2011) Aqueous partitioning of minor actinides by different processes. Sep Purif Rev 40:43–76
13. Whittaker DM, Griffiths TL, Helliwell M, Swinburne AN, Natrajan LS, Lewis FW, Harwood LM, Parry SA, Sharrad CA (2013) Lanthanide speciation in potential SANEX and GANEX actinide/lanthanide separations using tetra-N-donor extractants. Inorg Chem 52:3429–3444
14. Modolo G, Wilden A, Daniels H, Geist A, Magnusson D, Malmbeck R (2013) Development and demonstration of a new SANEX partitioning process for selective actinide(III)/lanthanide(III) separation using a mixture of $CyMe_4$BTBP and TODGA. Radiochim Acta 101:155–162
15. Bhattacharyya A, Mohapatra PK, Manchanda VK (2007) Solvent extraction and extraction chromatographic separation of Am^{3+} and Eu^{3+} from nitrate medium using Cyanex® 301. Solvent Extr Ion Exch 25:27–39
16. Bhattacharyya A, Mohapatra PK, Ansari SA, Raut DR, Manchanda VK (2008) Separation of trivalent actinides from lanthanides using hollow fiber supported liquid membrane containing Cyanex-301 as the carrier. J Membr Sci 312:1–5
17. Panak PJ, Geist A (2013) Complexation and extraction of trivalent actinides and lanthanides by triazinylpyridine N-Donor ligands. Chem Rev 113:1199–1236
18. Weigl M, Geist A, Mullich U, Gompper K (2006) Kinetics of americium(III) extraction and back extraction with BTP. Solvent Extr Ion Exch 24:845–860
19. Kaltsoyannis N (2013) Does covalency increase or decrease across the actinide series? Implications for minor actinide partitioning. Inorg Chem 52:3407–3413
20. Guillaumont D (2006) Actinide(III) and lanthanide(III) complexes with nitrogen ligands: counterions and ligand substituent effects on the metal-ligand bond. Theochem J Mol Struct 771:105–110
21. Nilsson M, Andersson S, Ekberg C, Foreman MRS, Hudson MJ, Skarnemark G (2006) Inhibiting radiolysis of BTP molecules by addition of nitrobenzene. Radiochim Acta 94:103–106
22. Takeshita K, Matsumura T, Nakano Y (2008) Separation of americium(III) and europium(III) by thermal-swing extraction using thermosensitive polymer gel. Prog Nucl Energy 50:466–469
23. Bhattacharyya A, Mohapatra PK, Roy A, Gadly T, Ghosh SK, Manchanda VK (2009) Ethyl-bis-triazinylpyridine (Et-BTP) for the separation of americium(III) from trivalent lanthanides using solvent extraction and supported liquid membrane methods. Hydrometallurgy 99:18–24
24. Matsumura T, Matsumura K, Morita Y, Koma Y, Sano Y, Nomura K (2011) Separation of trivalent minor actinides from fission products using single R-BTP column extraction chromatography. J Nucl Sci Technol 48:855–858
25. Van Hecke K, Modolo G (2004) Separation of actinides from low level liquid wastes (LLLW) by extraction chromatography using novel DMDOHEMA and TODGA impregnated resins. J Radioanal Nucl Chem 261:269–275
26. Bhattacharyya A, Mohapatra PK, Gadly T, Ghosh SK, Raut DR, Manchanda VK (2011) Extraction chromatographic study on the separation of Am^{3+} and Eu^{3+} using ethyl-BTP as the extractant. J Radioanal Nucl Chem 288:571–577
27. Mohapatra P, Sriram S, Manchanda V, Badheka L (2000) Uptake of metal ions by extraction chromatography using dimethyl dibutyl tetradecyl-1,3-malonamide (DMDBTDMA) as the stationary phase. Sep Sci Technol 35:39–55

28. Liu RQ, Wei YZ, Tozawa D, Xu YL, Usuda S, Yamazaki H, Ishii K, Sano Y, Koma Y (2011) Evaluation study on properties of a macroporous silica-based CMPO extraction resin to be used for minor actinides separation from high level liquid waste. Nucl Sci Technol 22:18–24
29. Liu RQ, Wei YZ, Xu YL, Usuda S, Kim S, Yamazaki H, Ishii K (2012) Evaluation study on properties of *iso*hexyl-BTP/SiO_2-P resin for direct separation of trivalent minor actinides from HLLW. J Radioanal Nucl Chem 292:537–544
30. Usuda S, Wei Y, Xu Y, Li Z, Liu R, Kim S, Wakui Y, Hayashi H, Yamazaki H (2012) Development of a simplified separation process of trivalent minor actinides from fission products using novel R-BTP/SiO_2-P adsorbents. J Nucl Sci Technol 49:334–342
31. Wei YZ, Sabharwal KN, Kumagai M, Asakura T, Uchiyama G, Fujine S (2000) Preparation of novel silica-based nitrogen donor extraction resins and their adsorption performance for trivalent americium and lanthanides. J Nucl Sci Technol 37:1108–1110
32. Wei Y, Kumagai M, Takashima Y, Modolo G, Odoj R (2000) Studies on the separation of minor actinides from high-level wastes by extraction chromatography using novel silica-based extraction resins. Nucl Technol 132:413–423
33. Wei YZ, Hoshi H, Kumagai M, Asakura T, Morita Y (2004) Separation of Am(III) and Cm(III) from trivalent lanthanides by 2,6-bistriazinylpyridine extraction chromatography for radioactive waste management. J Alloys Compd 374:447–450
34. Liu RQ, Wang XP, Wei YZ, Shi WQ, Chai ZF (2014) Evaluation study on a macroporous silica-based *iso*hexyl-BTP adsorbent for minor actinides separation from nitric acid medium. Radiochim Acta 102:93–100
35. Gorden AEV, DeVore MA, Maynard BA (2013) Coordination chemistry with *f*-element complexes for an improved understanding of factors that contribute to extraction selectivity. Inorg Chem 52:3445–3458
36. Bozic D, Stankovic V, Gorgievski M, Bogdanovic G, Kovacevic R (2009) Adsorption of heavy metal ions by sawdust of deciduous trees. J Hazard Mater 171:684–692
37. Semerjian L (2010) Equilibrium and kinetics of cadmium adsorption from aqueous solutions using untreated Pinus halepensis sawdust. J Hazard Mater 173:236–242
38. Javadian H, Ghaemy M, Taghavi M (2014) Adsorption kinetics, isotherm, and thermodynamics of Hg^{2+} to polyaniline/hexagonal mesoporous silica nanocomposite in water/wastewater. J Mater Sci 49:232–242
39. Dikici H, Saltali K, Bingolbali S (2010) Equilibrium and kinetics characteristics of copper (II) sorption onto gyttja. Bull Environ Contam Toxicol 84:147–151
40. Hanafiah M, Zakaria H, Ngah WSW (2009) Preparation, characterization, and adsorption behavior of Cu(II) ions onto alkali-treated weed (imperata cylindrica) leaf powder. Water Air Soil Pollut 201:43–53
41. Ozeroglu C, Metin N (2012) Adsorption of uranium ions by crosslinked polyester resin functionalized with acrylic acid from aqueous solutions. J Radioanal Nucl Chem 292:923–935
42. Salam MA (2013) Removal of heavy metal ions from aqueous solutions with multi-walled carbon nanotubes: kinetic and thermodynamic studies. Int J Environ Sci Technol 10:677–688